united nations educational, scientific and cultural organization

international atomic energy agency

the **abdus salam** international centre for theoretical physics

H4.SMR/1519-45

"Seventh Workshop on Non-Linear Dynamics and Earthquake Prediction"

29 September - 11 October 2003

Boolean Delay Equations (BDEs) as Succinct Models for Climate, Evolution, Earthquakes and other Complex Stuff

Climate Applications

M. Ghil

Ecole Normale Supérieure, France
& UCLA, USA

Feedback loops for "Great Salinity Anomaly"

GSA: Low-salinity water mass;
travelled cyclonically around subpolar North Atlantic,
1968 - 82, at 3 cms^{-1}

(Dickson *et al.*, 1988, *Prog. Oceanogr.*, **20**, 103–157)

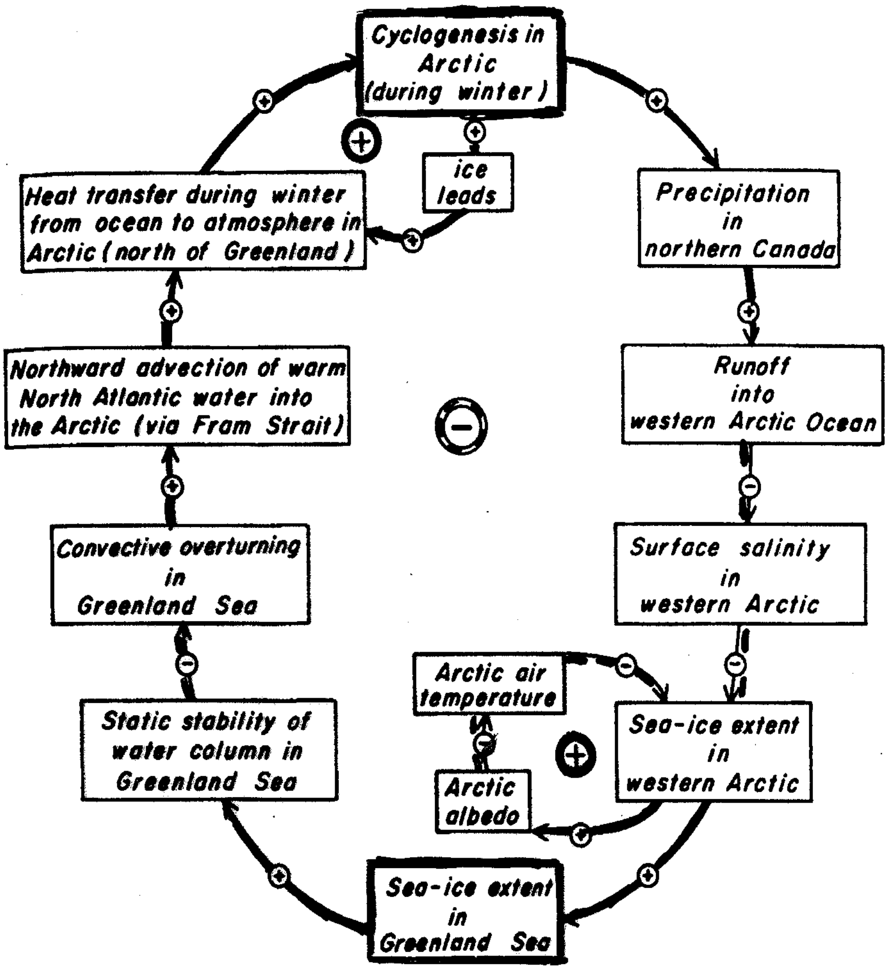

Mysak *et al.* (1990), *Climate Dyn.*, **5**, 111–133.

Model Equations

$$P(t) = C(t - \tau_1),$$

$$S_w(t) = \overline{P}(t - \tau_2),$$

$$I_w(t) = \overline{S}_w(t - \tau_3),$$

$$S_G(t) = S_w(t - \tau_4),$$

$$I_G(t) = I_w(t - \tau_5) \vee \overline{S}_G(t - \tau_6),$$

$$C(t) = S_G(t - \tau_7) \wedge \overline{I}_G(t) \wedge \overline{I}_G(t - \tau_8).$$

Reduction to a single BDE

$$\overline{S}_G(t) = S_G(t - \theta_1) \wedge S_G(t - \theta_2) \wedge .... \wedge S_G(t - \theta_5),$$

where $\theta_{1,2} = \tau_1 + \tau_2 + \tau_4 + \tau_{7,6}$; $\theta_3 = \tau_1 + \tau_2 + \tau_3 + \tau_5$;

$\theta_4 = \theta_6 + \tau_8$; and $\theta_5 = \theta_3 + \tau_8$.

Integer delays (whole years) $\Rightarrow$ periodic solutions.

The five θ_i represent travel time around each one of the 5 loops in Fig. 1.

Numerically, fundamental period

$$\theta = \theta_i + \theta_j,\ i, j \in \{1, 2, ..., 5\}.$$

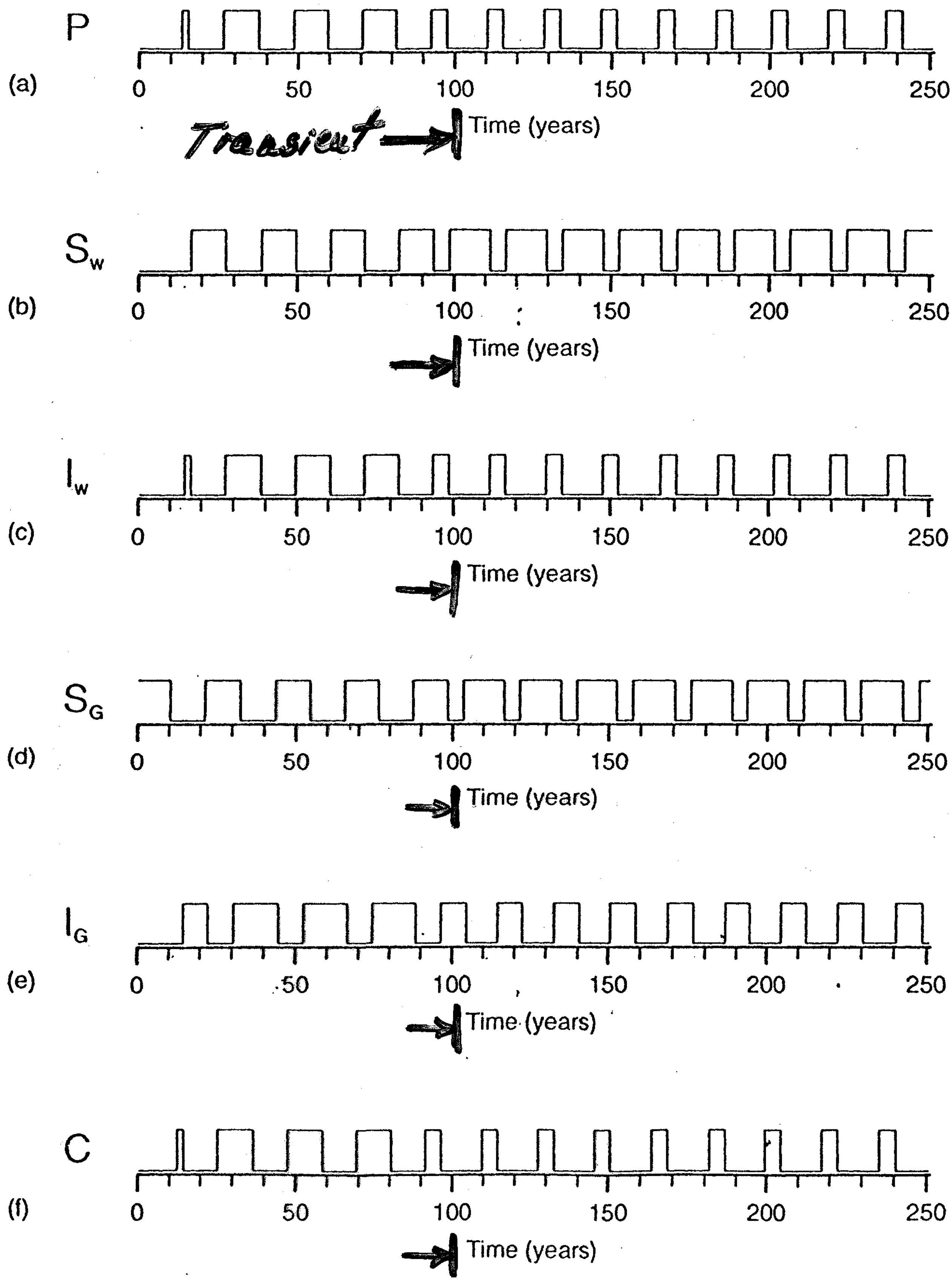

Figure 2 A simple solution with two jumps in each period for (a) P, (b) S_w, (c) I_w, (d) S_G, (e) I_G and (f) C using $T_F = 22$ and $\phi = 20$. The lags employed are given in (10). The period of the solution is 18 years.

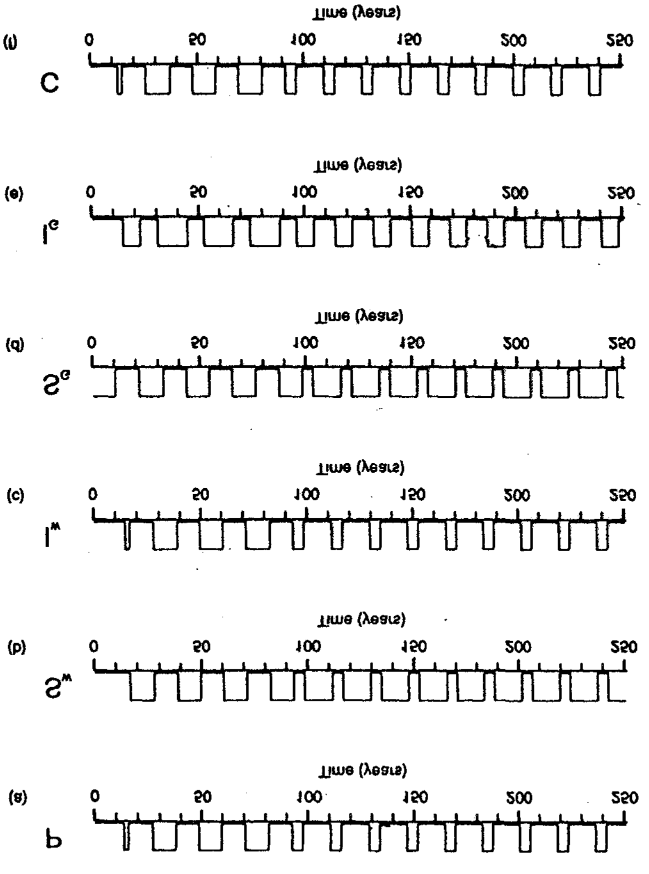

Fig. 2a–f. A simple solution with two jumps in each period for a P; b S_w; c I_w; d S_G; e I_G and f C using $T_F = 22$ and $\phi = 20$. The lags employed are given in (10). The period of the solution is 18 years

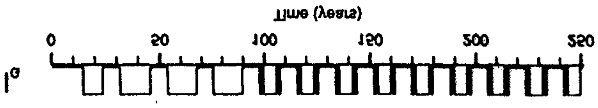

Fig. 3. The solution for I_G using $T_F = 22$ and $\phi = 21$ in (9). The period of the solution is still 18 years, but the complexity of the solution has increased. The other variables also have six jumps in each 18 year period

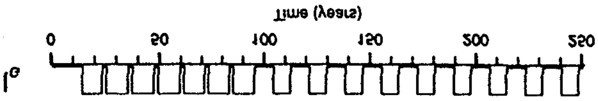

Fig. 4. The solution for I_G using $\tau_7 = 0$, $\tau_5 = 2$, $T_F = 12$ and $\phi = 0$. The period of the solution is 17 years

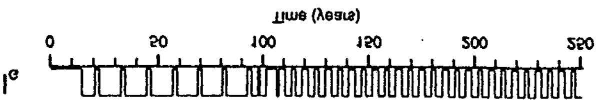

Fig. 5. The solution for I_G using $\tau_7 = 0$, $\tau_5 = 2$, $T_F = 12$ (as in Fig. 4) but $\phi = 9$. The period of the solution is now 11 years

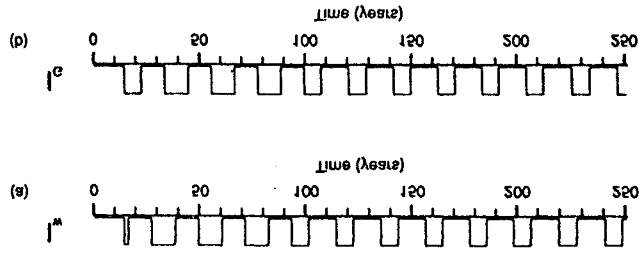

Fig. 6a, b. The solutions for a I_w; and b I_G; for $\tau_5 = 6$ and, as in Fig. 2, $T_F = 22$ and $\phi = 20$. The period is 21 years. Notice that, unlike Fig. 2, the fraction of a period for which ice is high is the same for both I_w and I_G

so that there are six jumps in each 18 year period. However, as in Fig. 2(e), the solution for I_G is characterized by roughly equal durations of a high ice state alternating with a low ice state.

Figures 4 and 5 are examples of solutions where the period is initial condition dependent (one period is not a harmonic of the other). Employing new lags $\tau_7 = 0$ and $\tau_5 = 2$ for which $\theta_1 = 7$, $\theta_2 = 8$, $\theta_3 = 4$, $\theta_4 = 13$ and $\theta_5 = 9$, initial period $T_F = 12$, and changing the phase of the initial condition ($\phi = 0$ in Fig. 4 and $\phi = 9$ in Fig. 5) the period of the solution changes from 17 ($\theta_3 + \theta_4$) to 11 ($\theta_1 + \theta_3$) years.

Finally, Fig. 6 demonstrates that the difference in times taken for low S_w to produce high I_G via the two mechanisms is responsible for the lengthening of the time of the high I_G relative to that of high I_w. By choosing $\tau_5 = 6$ (twice the control value) we find $\tau_4 + \tau_6 = \tau_3 + \tau_5 = 6$ years, and hence the routes via ice dynamics and ocean advection from S_w to I_G take the same time. Now $I_w = 1$ and $I_G = 1$ for 8 years in each 21 year period, with I_w leading I_G by 6 years.

We now investigate statistically the dependence of certain interesting solution features on the lags. For each of four different sets of lags, 500 experiments using random initial conditions were performed and the 'average' solutions were computed. For a quantity of interest f, we use $\langle f \rangle$ to denote a sum over a period (after transients have died away) and $\overline{f}$ to denote an average over the 500 random experiments. Therefore $\overline{\langle J \rangle}$ is the average number of jumps per period based on the 500 experiments and $\overline{\langle I_G = 1 \rangle}$ is the average number per period of high ice years in the Greenland Sea.

The first three sets of lags in Table 1 correspond to those used in Figs. 2, 4 and 6 respectively. In the final set of lags we take $\tau_2 = 2$ in order to demonstrate the extra period lengthening effect of varying a lag which is common to each of the θ_is (which give the times taken to go around the feedback loop). Only the set of lags corresponding to Fig. 4 exhibits a period dependence on initial conditions.

Notice that, as expected, $\overline{\langle I_w = 1 \rangle / \langle I_G = 1 \rangle} < 1$ except for the case corresponding to Fig. 6. There is a bias towards $\overline{\langle I_G = 1 \rangle / \langle I_G = 0 \rangle} < 1$ which originates from (6) which states that a $C = 1$ state cannot occur if a positive Greenland Sea ice anomaly has recently melted. To determine whether this bias of I_G towards the negative anomaly state is realistic, a long time-series of Green-

Statistics of solutions $\underline{J}$: no. of jumps per period

τ_2	τ_5	τ_7	$\overline{\underline{T}}$	$\overline{\left(\frac{< I_G = 1 >}{< I_G = 0 >}\right)}$	$\overline{\left(\frac{< I_w = 1 >}{< I_G = 1 >}\right)}$	$\overline{\underline{< J >}}$
1	3	1	18	0.69	0.68	7.32
1	2	0	14.9	0.99	0.5	4.78
1	6	1	21	0.75	1	9.78
2	3	1	20	0.98	0.66	8.15

Table 1 Average solution properties derived from 500 random initial states ~~condition experiments~~ employing the basic BDE model (1)-(6). The first line corresponds to the control set of values for τ_2, τ_5, τ_7 (see equation (10)).

$\langle\cdot\rangle$ Average over one period

$\overline{(\ )}$ - random initial states

τ_2	τ_5	τ_7	$\overline{\underline{T}}$	$\overline{\left(\frac{< I_G = 1 >}{< I_G = 0 >}\right)}$	$\overline{\left(\frac{< I_w = 1 >}{< I_G = 1 >}\right)}$	$\overline{\underline{< J >}}$
1	3	1	18	0.8	0.625	2
1	2	0	17	0.89	0.5	2
1	6	1	21	0.61	1	2.03
2	3	1	20	0.81	0.67	2

Table 2 Average solution properties derived from 500 random initial states ~~condition experiments~~ employing the extended BDE model (12) and (13).

El Niño on the Devil's Staircase: A Pathway to Prediction?

M. Ghil

Atmospheric Sciences & IGPP, UCLA

Motivation

1. ENSO is regular: locked to the seasonal cycle; QB mode, low-frequency (QQ?) mode.

2. ENSO is irregular: warm events occur every 2—7 years (1—8 years, etc.?).

3. We thought we understood, but we can't predict!

4. What to do? Let's see !..

Joint work with N. Jiang, F.-f. Jin, C. L. Keppenne, J. D. Neelin, A. W. Robertson, & A. Saunders + C.-C. Ma & C. R. Mechoso (for coupled GCM & input from M. Ji, P. Schopf & M. Suarez.

http://www.atmos.ucla.edu/tcd

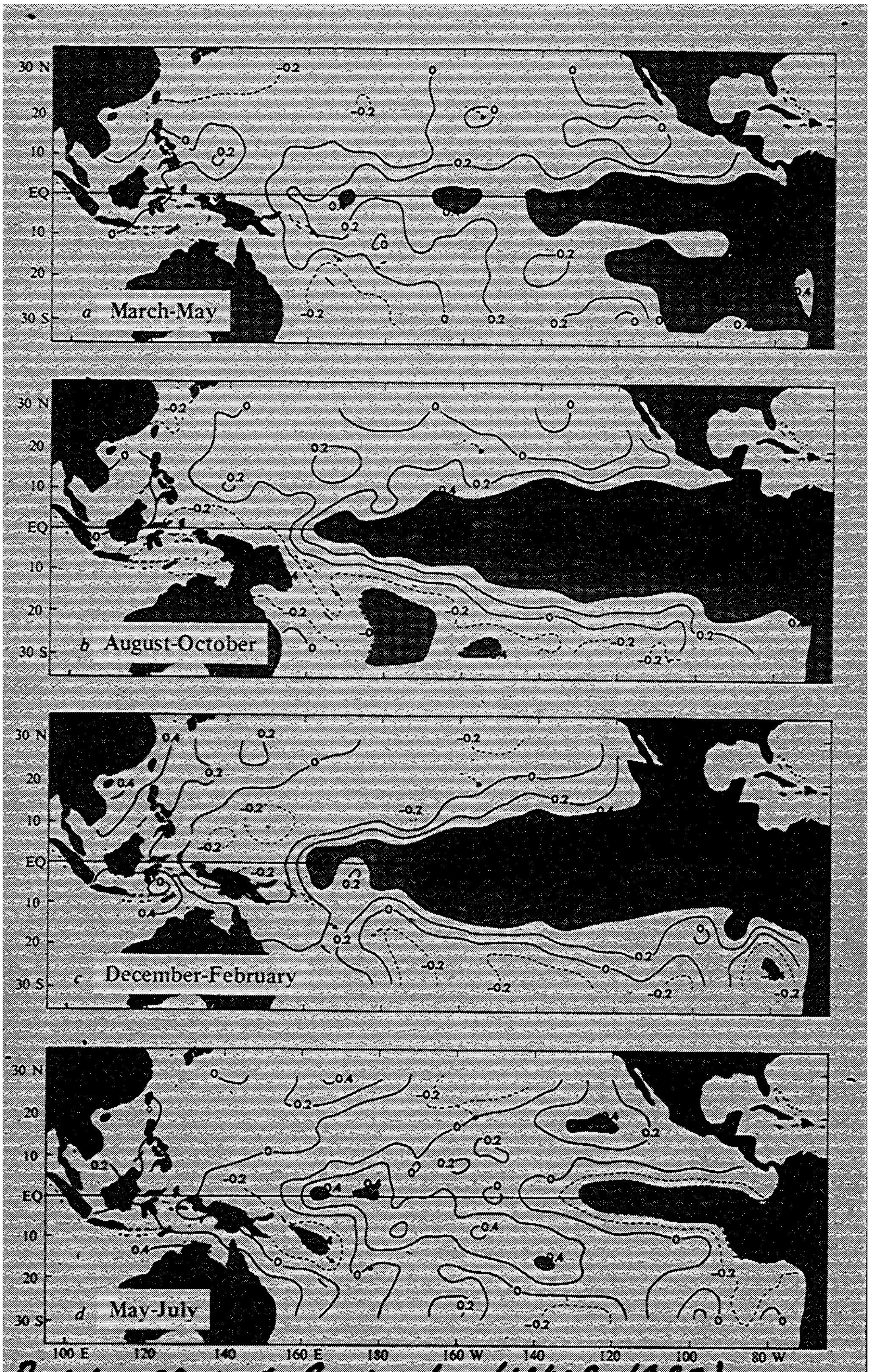

Rasmusson & Carpenter (MWR, 1982)

Scalar time series that capture ENSo

Southern oscillation: correlation of sea level pressure with that at Djakarta (Indonesia). Berlage (1957).

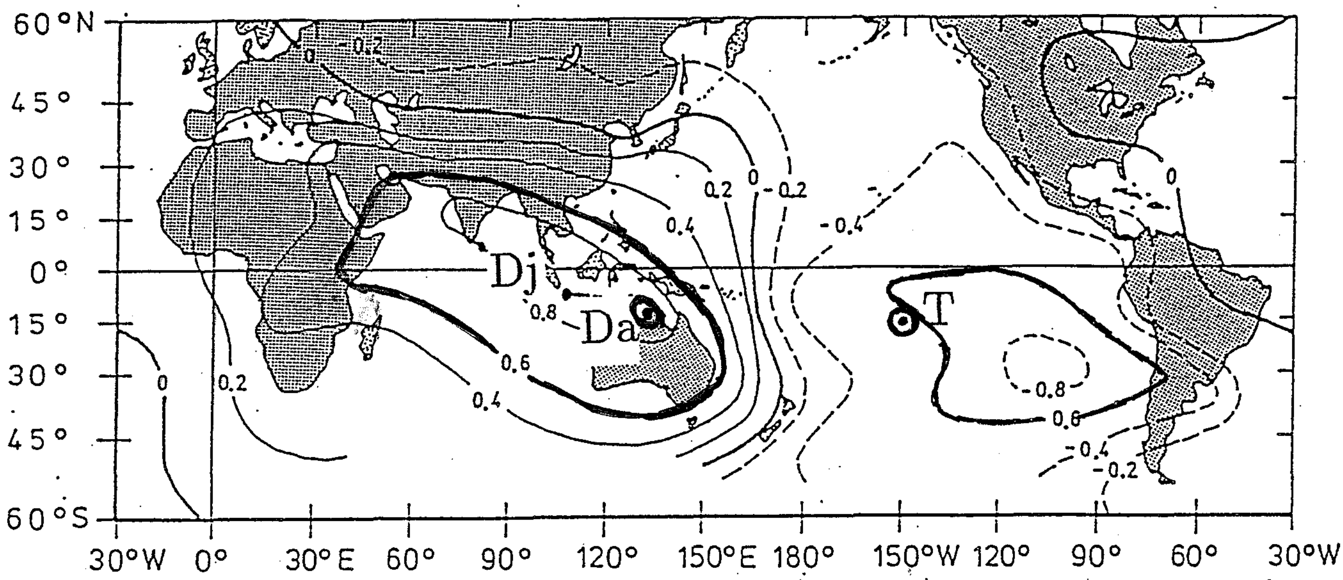

Time series of atmospheric pressure and SST indices

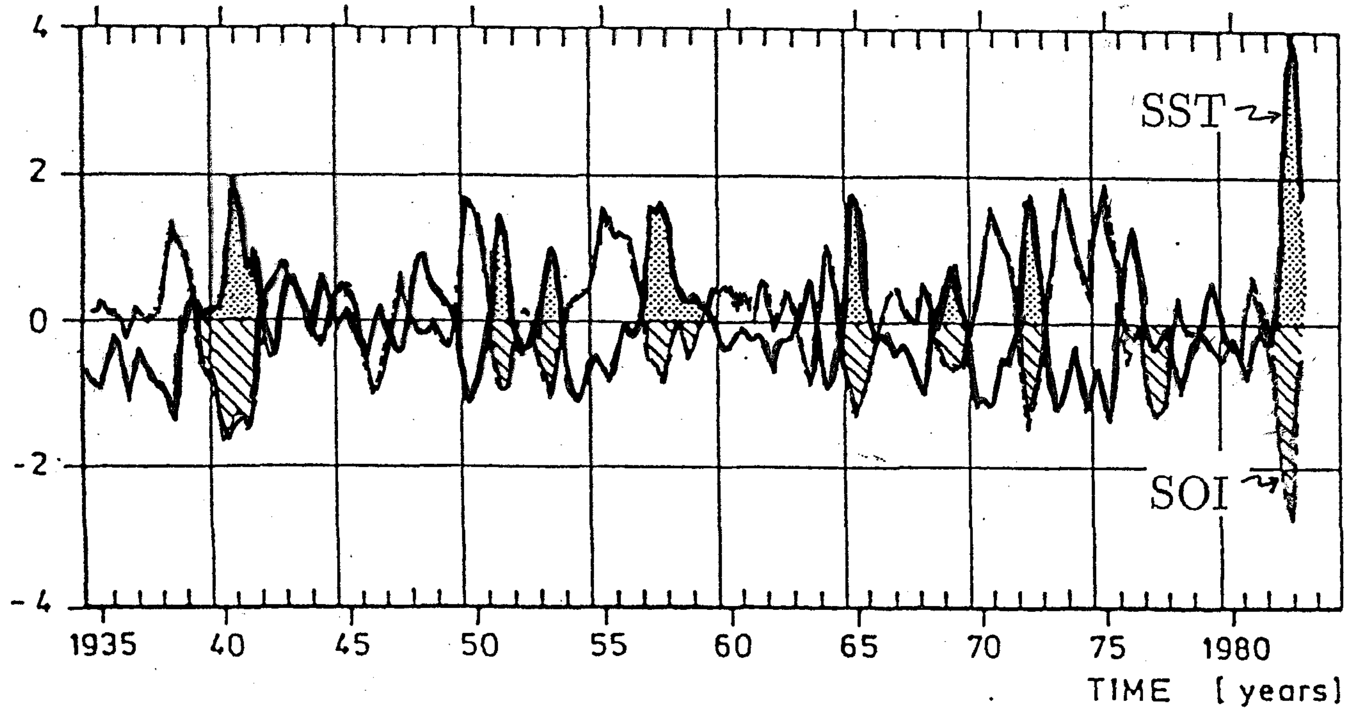

Figure 1 Time series of the Southern Oscillation Index, which measures the atmospheric sea-level pressure gradient across the tropical Pacific basin (*dashed curve*), and sea surface temperature (SST) anomalies at Puerto Chicama, Peru (*solid curve*). Both series are normalized by their standard deviation; shading indicates major ENSO warm phases (high SST, low Southern Oscillation Index). After Rasmusson (1984).

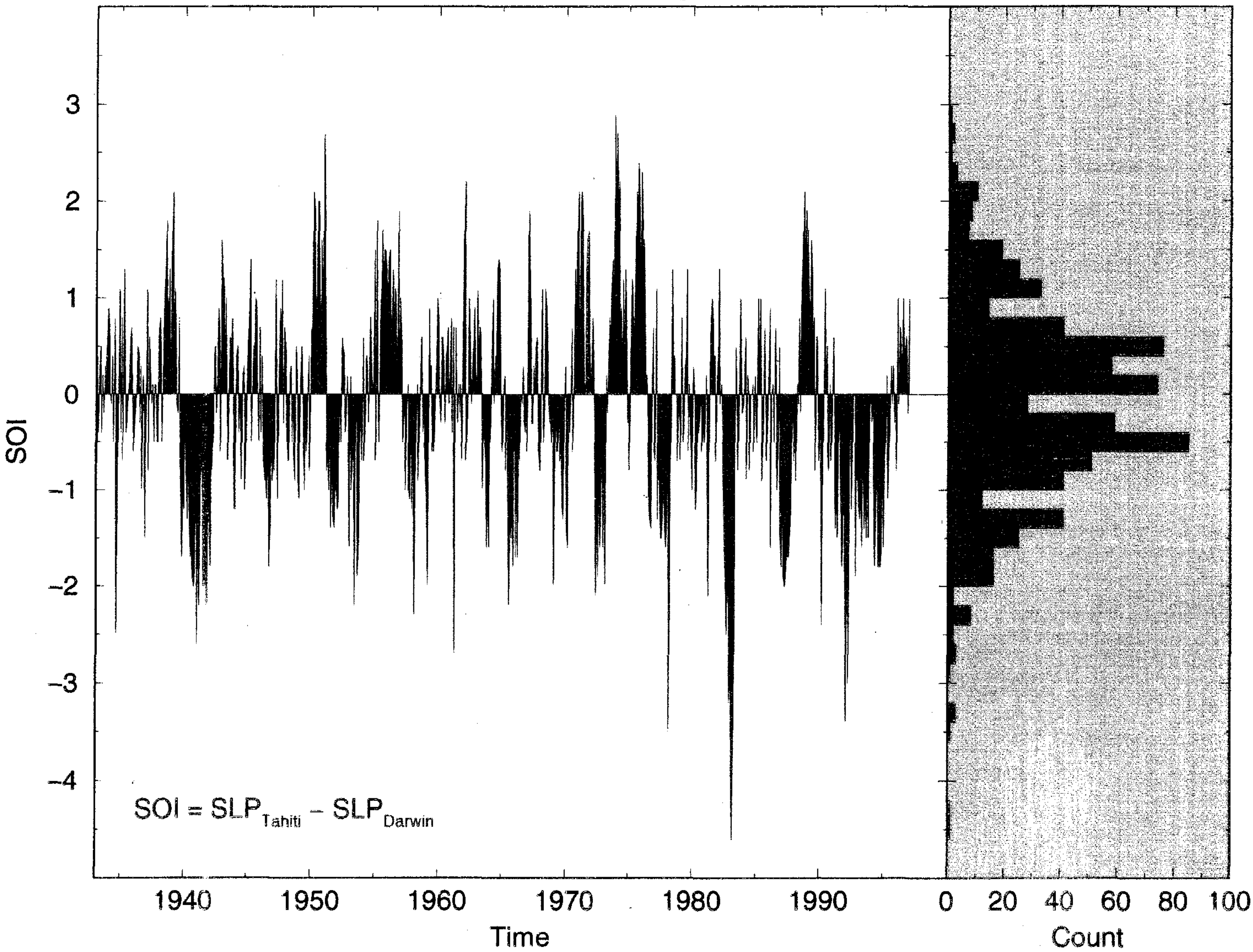

Courtesy of P. Yiou

Figure 1a: Model Scheme.

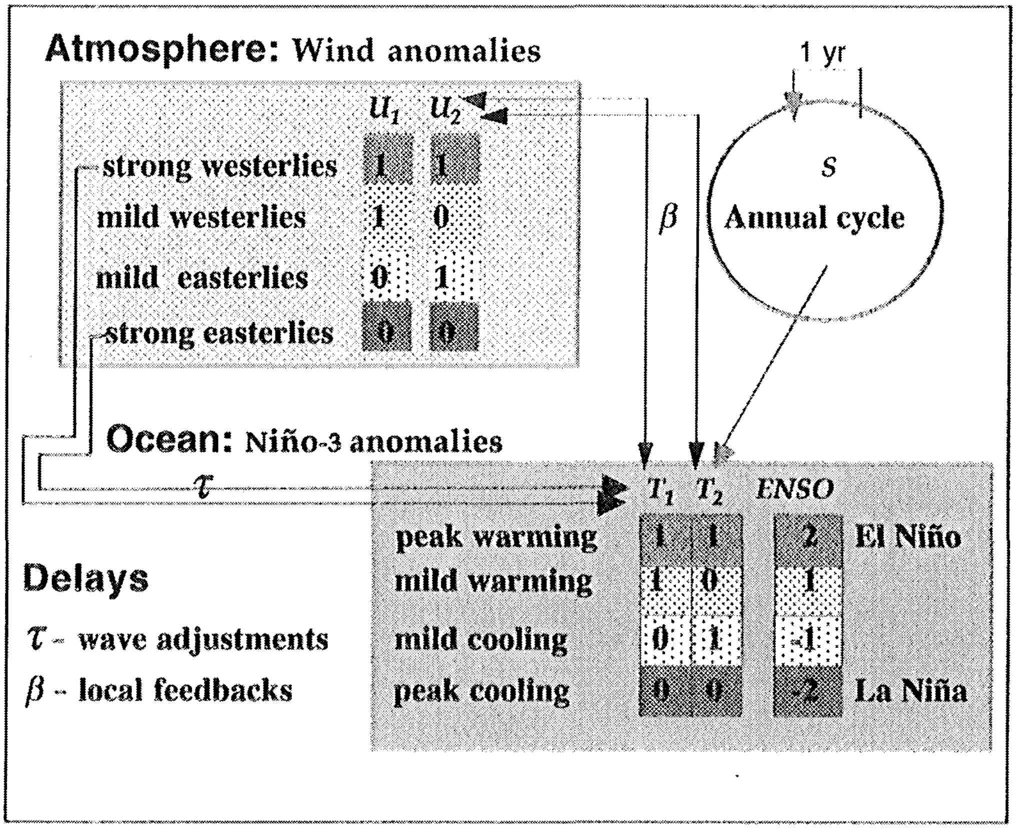

Saunders & Ghil (Physica D, 2001)

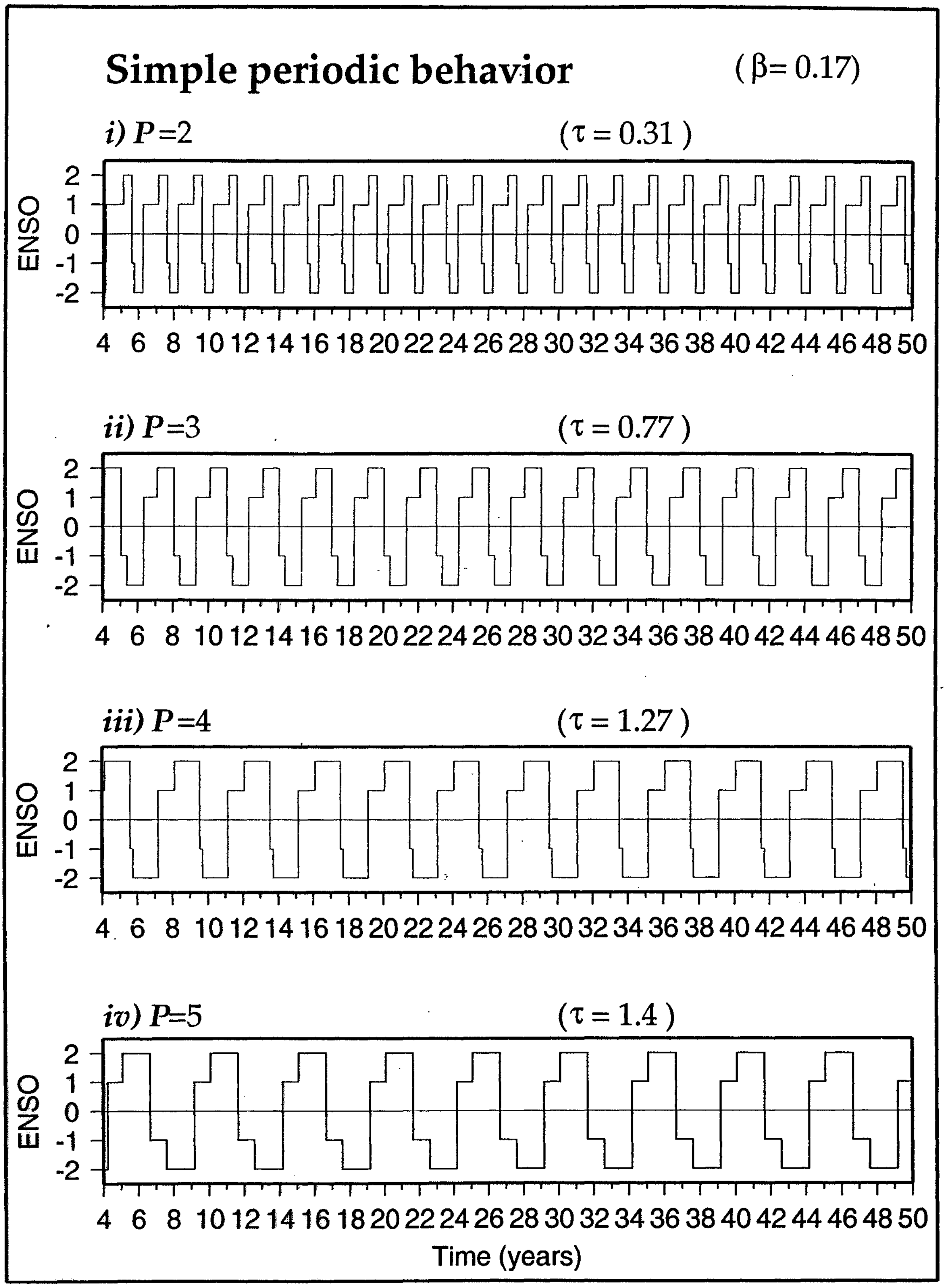

Figure 2a: Simple periodic behavior

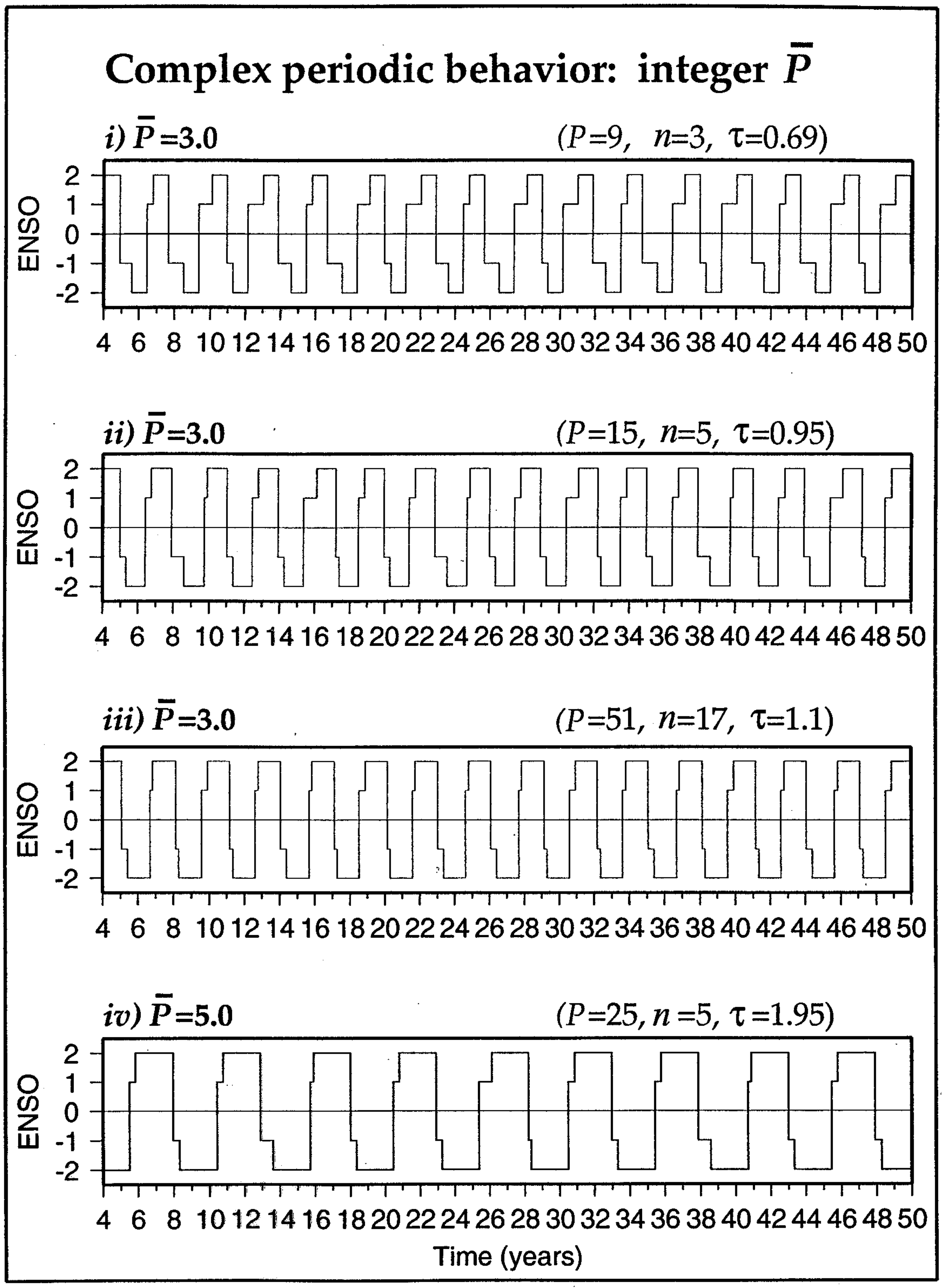

Figure 2b: Complex periodic behavior - integer average cycle length

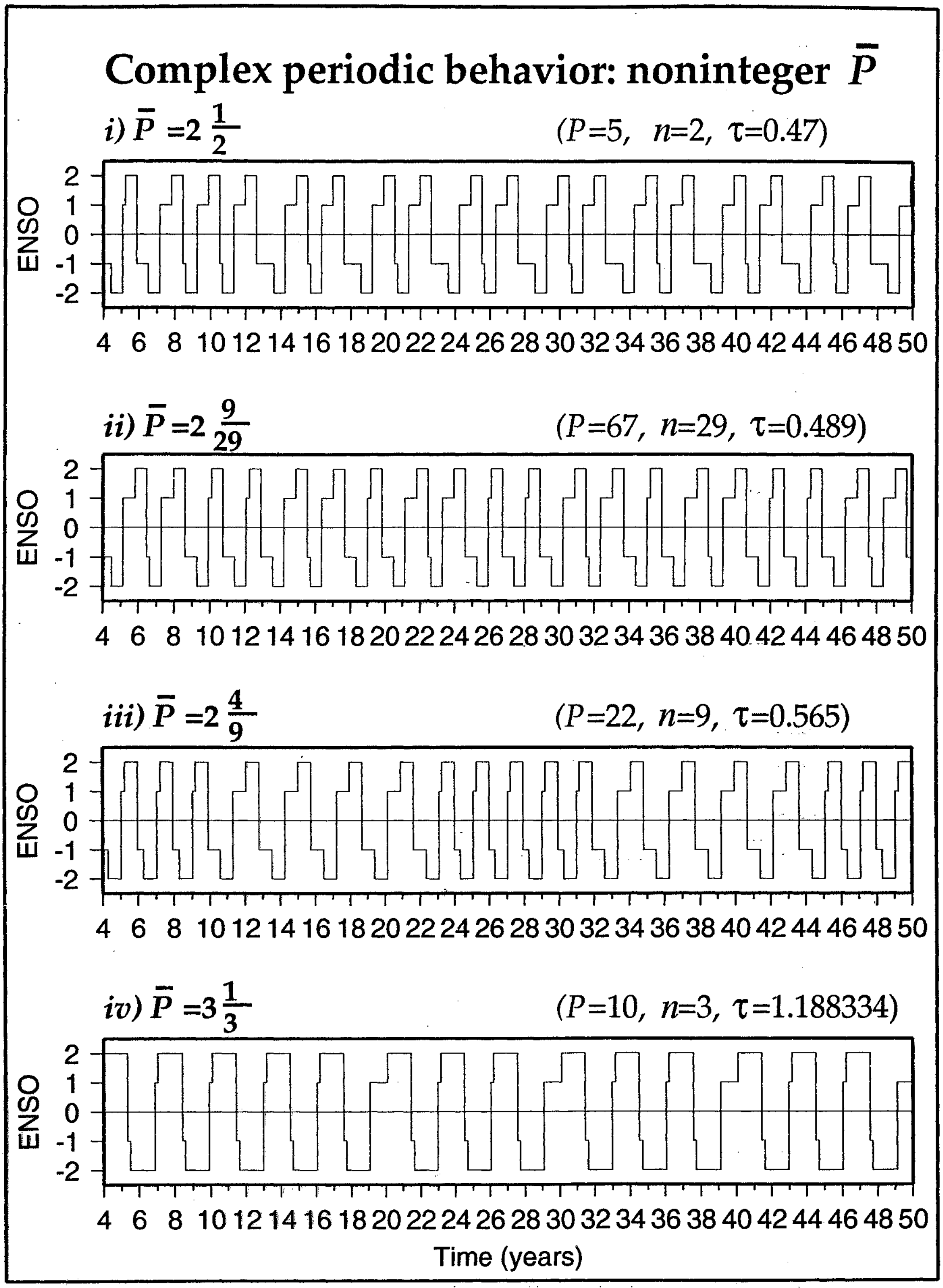

Figure 2c: Complex periodic behavior - noninteger average cycle length

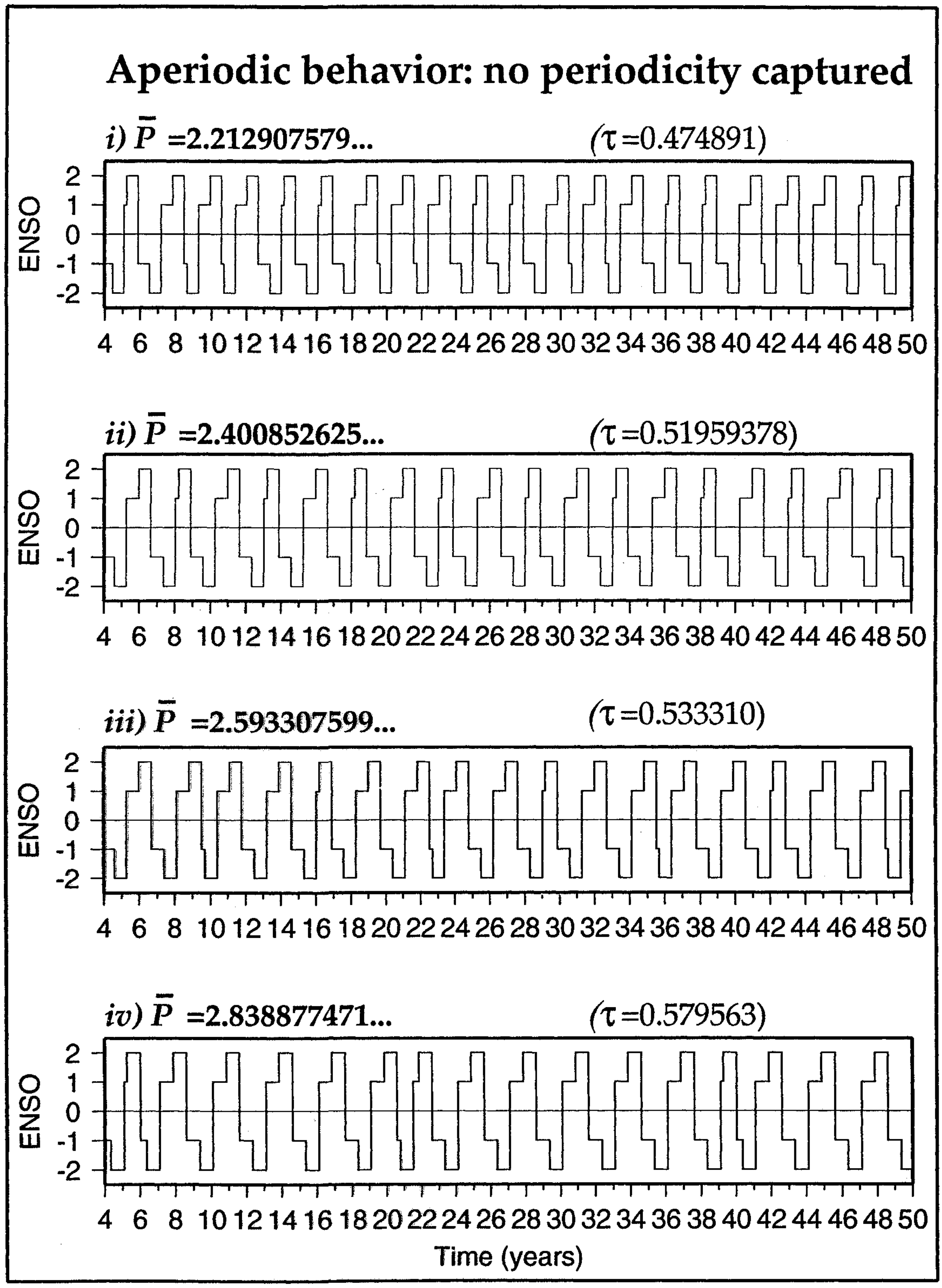

Figure 2d: Aperiodic behavior

Devil's staircase

(à la Jin *et al.*, '94; Tziperman *et al.*, '94; etc.)

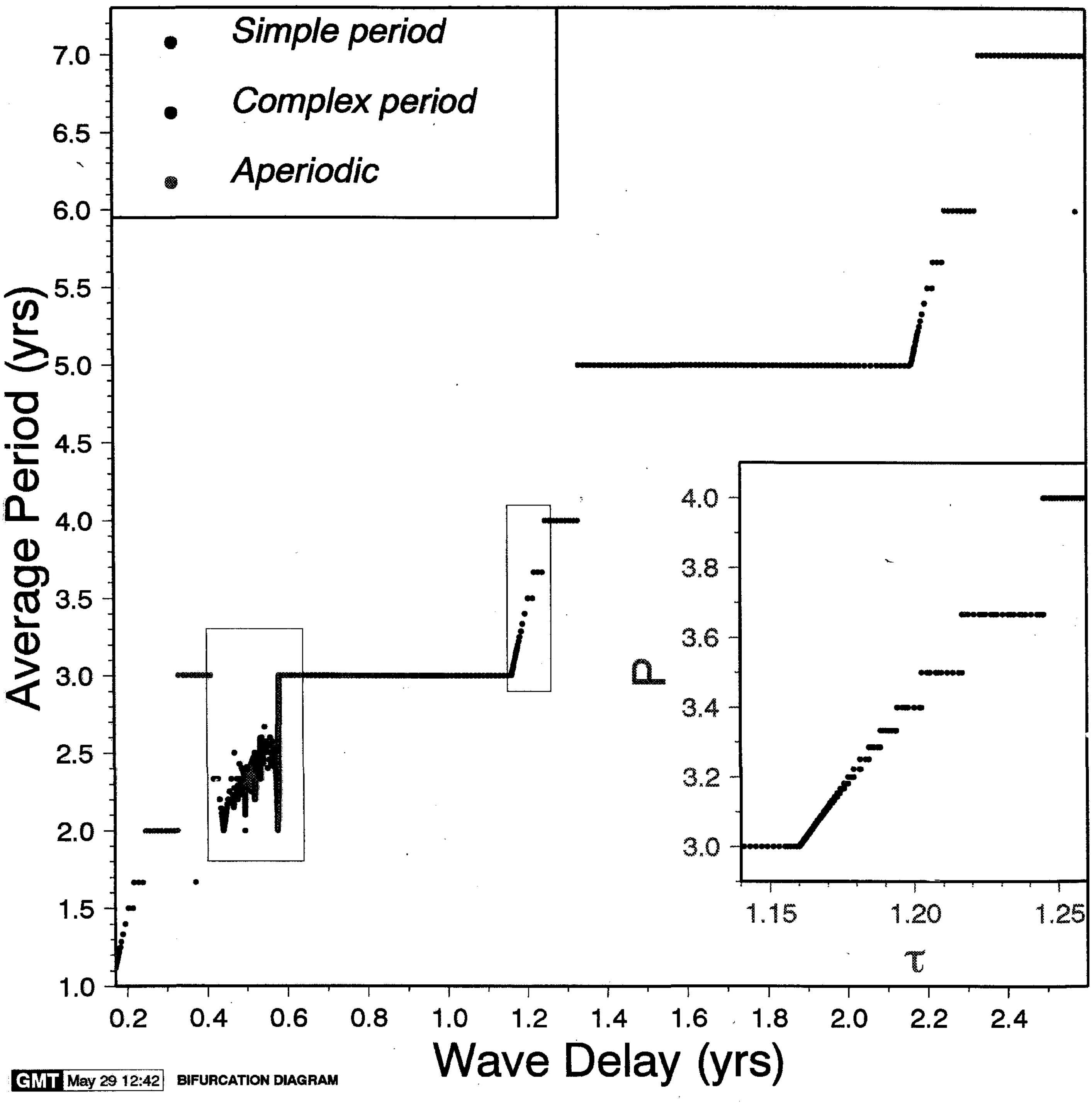

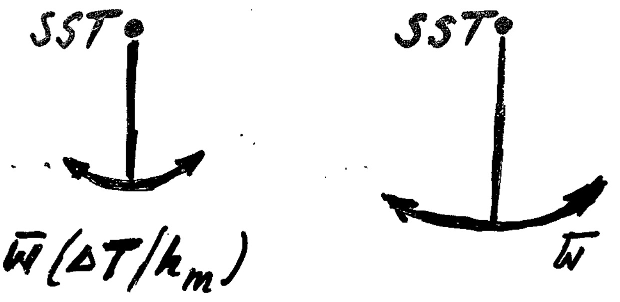

Eq'n for swing (pendulum)

$$\ddot{x} + \frac{g}{l}x = 0$$

Period $\frac{2\pi}{\omega_0} \sim \sqrt{l}$

Here "length" l depends on ΔT, etc.

$\Delta T = T(-h_m) - SST$

h_m = mixed-layer depth

The Devil's staircase

BETTMANN ARCHIVE

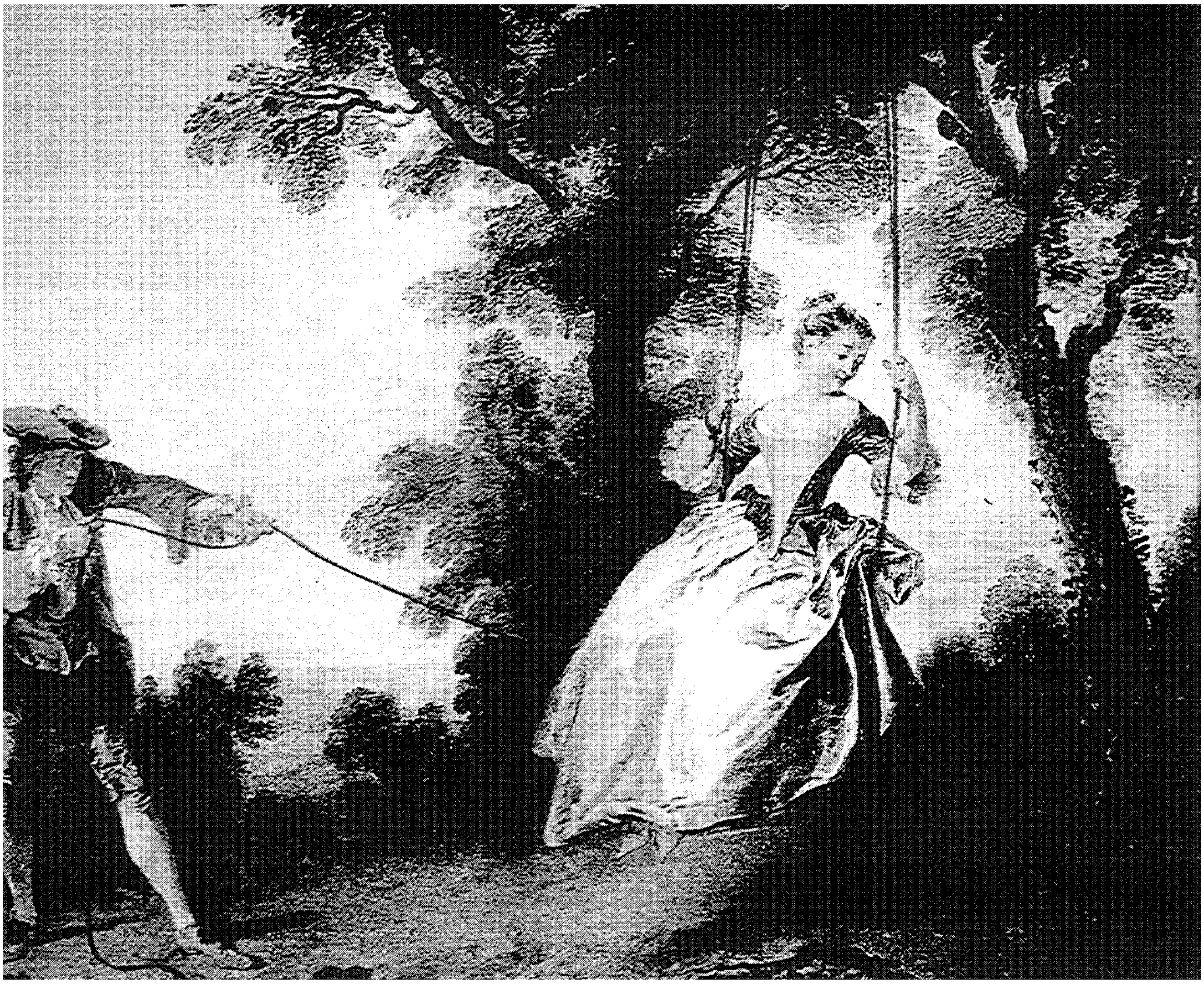

'The swing,' a painting by Nicholas Lancret, 1690–1743. The swing and attendant illustrate phase locking in systems containing two competing frequencies. Figure 1

P. Bak

Courtesy of F.-F. Jin & Cl. Périgaud

0031-9228 / 86 / 1200 38-08 / $01.00

PHYSICAL REVIEW B VOLUME 27, NUMBER 9 1 MAY 1983

Self-similarity and fractal dimension of the devil's staircase in the one-dimensional Ising model

R. Bruinsma
IBM T. J. Watson Research Center, Yorktown Heights, New York 10598

P. Bak
H. C. Ørsted Institute, DK-2100 Copenhagen Ø, Denmark

(Received 20 December 1982)

The one-dimensional Ising model with long-range antiferromagnetic interaction in an applied field is known to exhibit a complete devil's staircase in its $T=0$ phase diagram. In this Comment we discuss its self-similar properties and determine the fractal dimension.

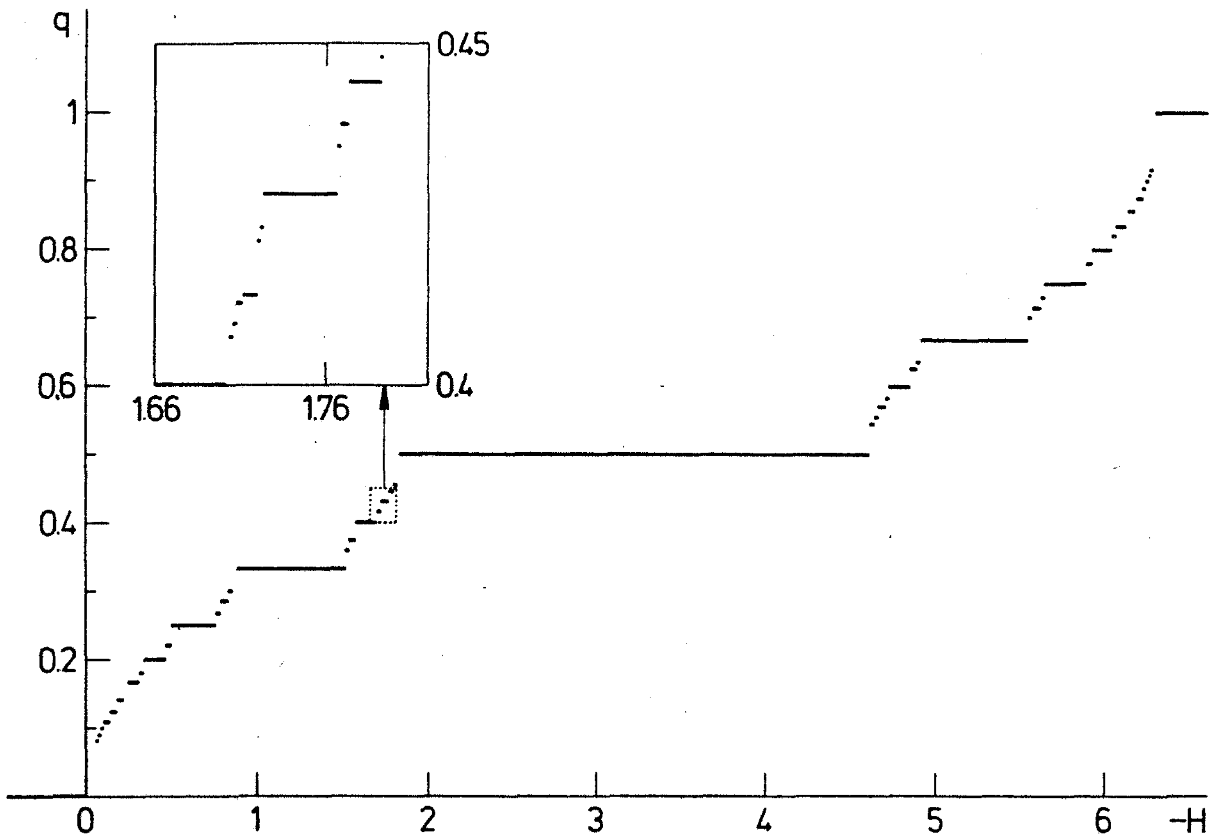

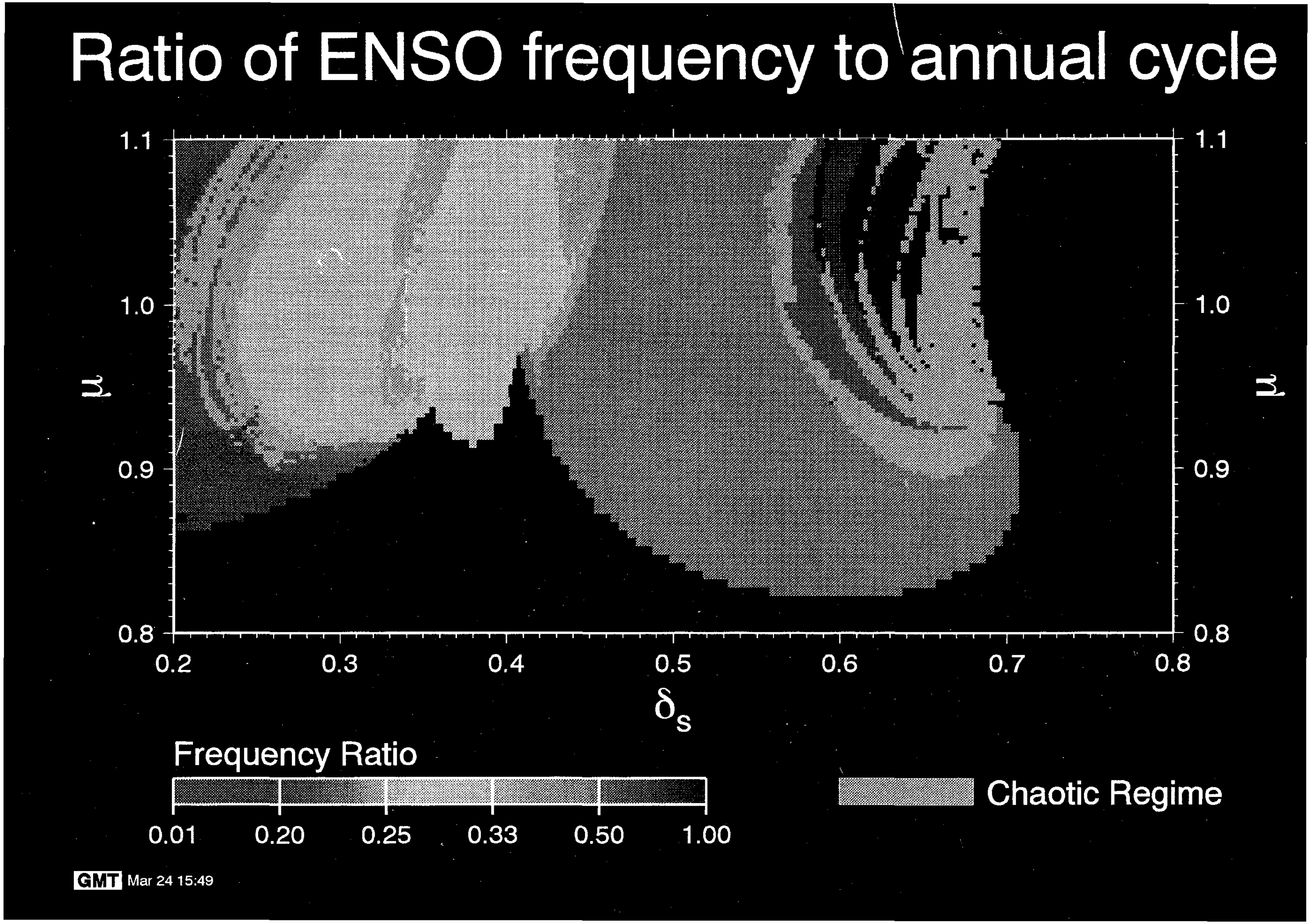
Ratio of ENSO frequency to annual cycle
1.1
1.0
0.9
0.8
μ
0.2
0.3
0.4
0.5
0.6
0.7
0.8
δs
Frequency Ratio
0.01
0.20
0.25
0.33
0.50
1.00
Chaotic Regime
GMT Mar 24 15:49

Devil's bleachers

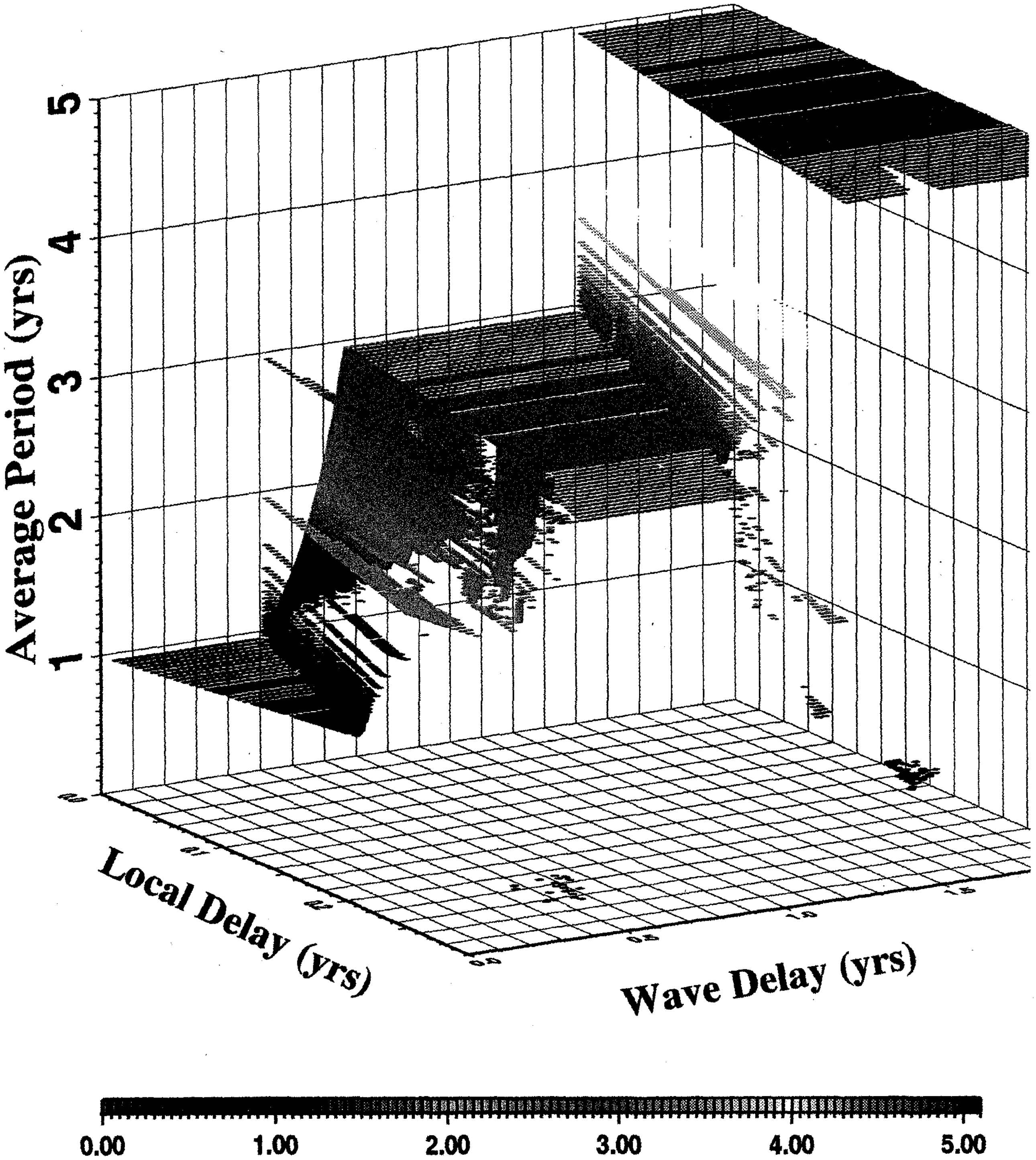

5 17:28 3D BIFURCATION DIAGRAM

Fractal Sunburst

= bizarre attractor in phase-parameter space